Delineation of groundwater potential in Southeastern Peshawar using lithostratigraphic properties and geophysical techniques

Asim Shahzad
Central South University
Hammad Tariq Janjuhah (hammadtariq013@gmail.com)
University Technology Petronas https://orcid.org/0000-0002-1522-5988
Syed Muzyan Shahzad
Central South University
George Kontakiotis
National and Kapodistrian University of Athens: Ethniko kai Kapodistriako Panepistemio Athenon
Meryam Fanidi
Central South University
Panayota Makri
National and Kapodistrian University of Athens: Ethniko kai Kapodistriako Panepistemio Athenon

Research Article

Keywords: Groundwater potential, electro-stratigraphy, vertical electrical resistivity (VER), pumping test, aquifer system, transmissivity, Dar Zarrouk parameters, formation resistivity, well logging, environmental monitoring

Posted Date: May 17th, 2022

DOI: https://doi.org/10.21203/rs.3.rs-1600618/v1

Abstract

The Peshawar basin is a part of the lower Himalayas that contains an enormous amount of groundwater storage. The evaluation of groundwater potential in the southern Peshawar district was done using a hydrogeological and geophysical technique. A total of 13 Vertical Electrical Sounding (VES) profiles were utilized to assess potential groundwater zones for surface resistivity studies. The aquifer system was delineated by comparing the data from five boreholes with the VES findings. It was also possible to find areas of super-saturated groundwater potential by linking metrics such as transmissivity (T), hydraulic conductivity (K), storativity (S), and the Dar Zarrouk. The examined aquifer is composed of clay, sand, gravels, boulders, and loose layers of lacustrine mud that are interlayered to form unconsolidated groundwater aquifer system. As a result, it is possible to use the aquifer for groundwater development because of its low-medium discharge.

1. Introduction

Water security has been monitored by scientists for a decade owing to decreasing global water supplies [1, 2]. The IPPC (2007, 2014, 2019) aims to promote water resource usage and subsurface water table stability for future generations. Water resource conflicts are linked to border disputes, major dams and reservoirs, environmental issues, and political identities [3]. Background knowledge of a region's geology and current hydrologic state is also critical for developing effective management techniques. Geophysical studies to evaluate the groundwater potential of confined and unconfined aquifers have become standard practice around the globe [4, 5]. Over the past several decades, rapid advances in electronic technology and numerical modeling have made geophysical research approaches for groundwater exploration and aquifer mapping much more feasible [6].

Hydrology, environmental geology, and geotechnical engineering all employ surface resistivity methods in various contexts [7–9]. Resistivity approaches are recommended to provide a high sample rate and high-quality data for precise target characterization in a geometrically constrained region with severe subsurface conditions. Electrical resistivity techniques are among the most widely used geophysical methods for groundwater evaluation due to their low cost, accessibility, and effectiveness in regions with highly diverse underlying lithologies [10–12]. According to Nag and Ray [13], GIS and remote sensing techniques are also used for groundwater assessment.

Geophysicists have found that combining drilling data with subsurface resistivity data may be highly advantageous since both hydraulic and electrical aquifer features rely on the pore spaces' structure [14]. Using geophysical data and the Vertical Electrical Sounding (VES) approach for near-surface measurement, the depth and thickness of an aquifer may be approximated with a degree of uncertainty. Calibration of VES data using borehole logs, lithologies and groundwater information enhance reliability [15]. Groundwater flow and aquifer potential in saturated situations may be determined using hydraulic characteristics calculated from pumping tests conducted in drilled boreholes [16]. However, if pumping experiments are not possible, it is feasible to get quantitative estimates of hydraulic characteristics by combining them with hydrogeological data [17].

Before drilling a borehole, it is also possible to optimize the site of wells to limit the chance of failure or unexpectedly low pumping rates [18]. The electrical resistivity approach has shown to be effective in groundwater identification and usage [19]. It includes extensive information on hydrogeological conditions and groundwater storage.

A physically significant correlation must be applied theoretically or experimentally to decode the aquifer's resistivity distribution into the aquifer Dar Zarrouk parameters [21, 22]. Aquifers containing fresh and saltwater in various regions can be resolved using longitudinal conductance (S), transverse resistance (TR), longitudinal resistivity (Rs), and coefficients of anisotropy (λ) [23, 24]. Several authors have already assessed Aquifer protection capability using Dar Zarrouk functions [25, 26]. Protective capacity measurements may reveal surface zones where pollutants are being transferred straight into an aquifer [27]. Multiple well-logging and pumping tests in boreholes (Tube wells) are important for estimating aquifer characteristics, including transmissivity (T), hydraulic conductivity (K), storage capacity (S), and the formation factor (F) [22]. The aquifer system is calibrated with the VES data using drill logs, borehole lithologies, groundwater information, and hydro-chemical data, enabling it to be better defined [26, 28].

In this study, an attempt has been made to define groundwater potential and map probable zones for fresh groundwater exploration by characterizing underlying lithologies to a depth of 170 m. This work included 13 VES, 5 boreholes, hydrologer data, and pumping tests, with the primary objective being to determine the subsurface lithologies and groundwater potential zone in the region. The underlying lithology, aquifer system, and Dar Zarrouk parameters were identified using the integration of VES, borehole, and hydrologer data sets. The transmissivity, hydraulic conductivity, and storativity of the aquifer system were estimated using the pumping test data.

2. Geology And Hydrology Of The Study Area

Because of the Indian-Eurasian plate collision, Pakistan's northern territory constantly undergoes deformation [29–31]. In this region, a large number of basins and valley systems. Massive amounts of weathering and erosional products have been transported across large distances and deposited in different sedimentary environments, such as talus slope, alluvial fan, and flood plain deposits [32, 33].

A sedimentary archive in northwest Pakistan's Peshawar Basin provides a record of the Pleistocene rock-debris supply pattern. The Pliocene–Pleistocene uplift of the Attock–Cherat Range in northern Pakistan prevented the Indus and Kabul rivers from draining, forming the intermountain Peshawar Basin 2.8 Ma ago [34, 35]. Late Pliocene sediment deposition rates ranged from 2 cm/1000 years to 15 cm/1000 years, with accumulations surpassing 300 m thick at the southern boundary (Burbank and Tahirkheli, 1985). To a large extent, alluvial fans that prograded from the neighbouring Attock–Cherat range along the southern boundary sank the basin. It has subsequently been fragmented by erosion to form the piedmont plains on the lower slopes of the alluvial fans. The inter-basin drainage networks (Kabul, Kalpani, and Indus rivers) ponded from a tectonically controlled drainage threshold (the Khairabad fault) at perhaps near Nizampur (Main Boundary Thrust fault) resulted in interbedded lacustrine and alluvial sediments (Fig. 1a). Ponding created low-energy floodplain and flood-

pond sediments in the basin's southwest and centre [33, 38]. Late Pleistocene lakes were considered to have deposited lacustrine sediments in the Peshawar basin [37]. However, the geomorphological (origin) properties of these sediments are rhythmically bedded flood deposits, which Cornwell [38] discovered after detailed research covering an area of 8300 km^2 in northern Pakistan. Whereas, river mud is covered with thick rhythmic glacial lake boulders in the southern portion of the basin, alluvial fan deposits are abundant, and the top section of the basin is covered with vertical and continuous loess deposits [34, 36, 37]. The Peshawar basin lies on the hanging wall of the Attock-Cherat Range north of the Main Boundary Thrust (Fig. 1a). The basin's north, northeast, and northwest are meta-sediments with Malakand-Swat-Bunair granitic intrusions. .

Furthermore, dolomite and limestone are found in the southwest, while exposed shales are in the southeast. Alluvial deposits are hydrogeological significant because of their inter-layered and diverse lithologies of clays, gravels, sands, and boulders. This alluvial deposit layer displays groundwater systems that are unconfined to semi-unconfined [33]. Several surface streams in the area are most active during the monsoon season, and the terrain of the studied region influences the subsurface water flow [39, 40].

The overburden comprises the top clays, sand, and alternating layers of sand gravel and mixed boulder strata. The research region is part of the Peshawar basin, and the Peshawar basin's stratigraphic sequence is typically occupied by sedimentary to metasedimentary rocks from the Precambrian to the Jurassic period [31, 41]. The Kabul River and the Bara River are the two primary rivers that recharge the aquifer systems. Previous hydrological estimations based on subsurface lithology of borehole data in the Peshawar basin had determined the aquifer systems (Tariq, 2001). Which deduced that the Peshawar valley would have plenty of water, which comes from glacier melts in the north and northwest regions and is used for drinking and irrigation [40, 42]. The principal source of recharge for the subsurface aquifer is rain-fed streams.

3. Materials And Methods

3.1 Electrical resistivity Data

A total of 13 VES sites were reported in the study region, ranging from 71.2–71.8 °E and 33.75–33.9°N (Fig. 1). The ABEM Terameter SAS-4000 instrument was used to gather data. For the VES survey, we employed a Schlumberger electrode arrangement with a maximum distance between current electrodes of 180–200 m [25, 26]. The data for apparent resistivity (a) gathered across the study region comprised half of the current electrode spacing (AB/2), voltage (V), current (I), and geometrical factor (G) in a typical N-S to E-W profile orientation (K). The apparent resistivity of the gathered field data was mechanized using computer software (IPI2win). Based on the thickness of the geoelectric layers, the data is interpreted into a model (Fig. 2). Resistivity data were assigned lithological units based on existing borehole lithology records and standardized resistivity measurements in the research region.

Dar Zarrouk parameters are described in electrical prospecting as the product of transverse unit resistance (T) and longitudinal conductance (S), as well as the coefficient of anisotropy (λ). These qualities are essential for data interpretation as well as stratified conductor modeling. According to the subsurface electro-stratigraphic model, these units are a quantitative product of apparent resistivity and thickness [22]. The hydraulic Dar Zarrouk is as follows:

$$Si = \sum_{i=1}^{n} \frac{hi}{pi} \quad (Siemens) \qquad (1)$$

$$\boldsymbol{Ti = \sum_{i=1}^{n} pi.hi \ (Ohm.m^2)} \qquad (2)$$

$$\lambda = \sqrt{\rho_T / \rho_L} = \sqrt{\frac{\left(\sum_i^n \rho_i h_i\right)\left(\sum_i^n \frac{h_i}{\rho_i}\right)}{\left(\sum_i^n h_i\right)^2}} \qquad (3)$$

Whereas *PT and PL* represent the transverse apparent and longitudinal apparent resistivity respectively, the equation for the coefficient of anisotropy may be easily obtained using a one-square-meter block of earth cut out of a set of layers of the infinite lateral extent of particular resistivity *p* and variable thickness of depth *h*, with the subscript *i* signifying the position of a layer of earth. Integrating VES data with borehole data sets for both confined and unconfined aquifer systems produced the thickness maps (Fig. 2).

3.2 Tube Well data and Pumping test analysis

In a recent investigation, five tube wells (PS-01, PS-02, PS-03, PS-04, and PS-05) were bored, each with a depth of 160–170 m and several borehole analyses were also performed (Fig. 1b, 3, 4, S1). Drilling findings reveal alluvial sediments as well as lacustrine mud as underlying lithologies in a few boreholes. The lithology, geometry, resistivity, formation factor, and specific yield of water-bearing rocks were determined using geophysical well logs, as well as the source, transport, and chemical and physical properties of groundwater [43]. This information was then shown to identify the saturated zone and the tube well design. Each well was pumped for more than 800 minutes, with the decline of the water level in the tube well and the discharge rate being measured (Table 1, [18, 44]). Field measurements were plotted on semi-logarithmic coordinate paper, with the drawdown (h) plotted on the linear y-axis scale and the time (t) after pumping began shown on the logarithmic x-axis scale (Fig. 3, A1). Transmissivity and hydraulic conductivity were calculated using the Cooper–Jacob method (single-well pumping test) [45]. The following is the equation that was used to calculate the Transmissivity:

While T (h0-h) is the drawdown per log cycle of time, Q is the constant pumping rat. Based on the pumping test analysis of the following formula, the hydraulic conductivity of stratified aquifer layers was determined [46].

K = T/d (5)

Where K stands for hydraulic conductivity, T for transmissivity, and d for saturated layer thickness (pumped depth). The resistivity and grain size of borehole lithologies were used to classify them. The studied depth and expected resistivity values were plotted against AB/2 until the depth and anticipated resistivity values were achieved. Drilling data from the VES transects were utilized to calibrate the anticipated resistivity and lithologies, as well as to identify prospective zones. The anticipated resistivity and lithologies were calibrated using existing drilling data from the VES transects' area (Fig. 2, 4, S1). Using resistivity modeled curves and borehole lithology, a standard strata correlation was produced separately for lithologies above and below the water table (Table 2). The resulting standard correlation was applied to every one of the field curves generated from all of the VES data points [25]. Most geophysical methodologies are difficult to comprehend because the response curves generated by resistivity data may be matched with various realistic resistivity distributions. As a consequence, a conclusive geological model may only be proposed once the data has been calibrated against a separate set of data collected separately. In the study area, lithostratigraphic logs, surface geological observations, water table depths, and electrical conductivities recorded in existing tube wells were used [47] (Fig. 2, 4).

3 Aquifer Model

The VES data, tube well data (usually the lithology), and hydrologic data sets were used to develop a complete three-dimensional model of the aquifer system in the research region [25, 48]. Based on three parameters data sets; surface resistivity values, litholog and the well logs of the tube well, a comparison was established with respect to the surface topography (Fig. 6). The lithologies defined aquifers as unconfined or confined, as well as the aquifers' development environment. Lithostratigraphic models of the thirteen VES values and the five-tube well were matched, and the types of aquifer system were determined..

4. Results

4.1 Electro-stratigraphic variation

Geo-electrical data was categorized by resistivity and layer thickness using quantitative analysis of vertical electrical soundings. These geo-electrical units were used to develop the electro-stratigraphic model. As a result, five to six geoelectric subsurface layered assemblages were identified. We gathered geophysical and geological data, as well as lithological data from tube wells, to construct a precise hydrogeological model by correlating and establishing a particular link between all variables [48, 49]. The groundwater subsurface model a series of consecutively low and high resistivity differences. We were able to determine the depth of the groundwater water table and distinguish between unsaturated and saturated sediments over the study area.

Although clay layers interlocked in the lithology of saturated sediments, many subsurface resistivity faces (21 ohm-m) have been identified, resistivity values fluctuate significantly (15–85 ohm-m) in unsaturated zones (Table 2, Fig. 2). VES sounding such as, VES-1, VES-4 and VES-7 illustrate interpreted preliminary findings employing the subsurface layers' thickness, resistivity, and lithology. The underlying groundwater distribution for each stratum is shown by compiling an electro-stratigraphic column (Fig. 2).

4.2 Aquifer parameters analysis

Characteristics of Dar-Zarrouk, such as transverse resistance (TR), longitudinal conductance (S), and coefficient of anisotropy (λ), were estimated for the aquifer system's cover layer (Table 3, Fig. 5). S is one of the geo-electrical measurements used to identify areas of potential groundwater [52]. By Hasan, *et al.* [53], aquifer system longitudinal conductance (S) refers to the protective capacity of layers above the aquifer that may operate as a filter/barrier for percolating fluid. According to the results, S values ranged from 0.14 to 1.2 mhos (Table 3). The S concentrations of 0.7 to 1.2 mhos have been found in the southeastern half of the study area. The high findings might be explained by the existence of clay beds, which are classified as having "Good" defensive properties (Table 4, Fig. 5b). There is a decent level of protection in the study area's central and northeastern regions with values between 0.29 and 0.65 mhos. Despite having a week to a poor protective capacity of 0.07–0.14 mhos, the area's Northwestern and Southwestern sides are nevertheless classified as having a week to bad protective capacity (Table 4).

The values of transverse resistance range from 2300 to 22948 Ωm² (Table 3, Fig. 5a). High TR values (10000–22000 Ωm²) may be found from the northwest to the southwest. The research area's low TR values (7000 Ωm²) are calculated in the middle southwestern section. Low T values, on the other hand, are associated with low-resistivity formations (such as clayed soil) and a shallow foundation, while higher T values are associated with high-resistivity formations and occurrences of deeper groundwater potential [52].

The coefficient of anisotropy can be used to determine the aquifer's type and storage capacity [6, 59]. Electrical anisotropy in rocks is produced in multilayered aquifers via alternating layers of thin-bedded sandstones and shales with apparent lamination [60]. The λ gives information on inhomogeneity in underlying materials like topsoil and worn layer. Inhomogeneity is also linked to water development [6, 24, 59]. It also connects water development with inhomogeneity, according to the study [24]. Between 0.27 to 1.35 was shown to be the optimum value of "λ" in recent research (Table 3). In the Northwestern section of the high "λ" values (> 1) are indicating the subsurface clay with minor sand dominating layers. There is a noticeable trend toward the northeastern part of the country in terms of low to intermediate "λ" (0.22–0.5) values (Fig. 5c).

The mixed lithologies of sand gravels and boulders, as well as the low coefficient of anisotropy associated with the fractured bed rocks material, are represented by intermediate anisotropy [61]. The low anisotropy also suggests high-density water-filled fractures in basement rocks [52], and although this research did not represent a particular basement complex, it was thought to be important for understanding groundwater potential.

The aquifer transmissivity, hydraulic conductivity, and formation resistivity are shown by Borehole Tube or well data (PS-01, PS-02, PS-03, PS-04, PS-05) (Table 1, Fig. 4, S1). By comparing geophysical logs, a correlation between surface electrical resistivity and borehole data was developed, and resistivities derived from VES were connected to borehole lithologies [51]. TR and aquifer transmissivity have a direct connection, with the greatest TR values correlating to the highest aquifer transmissivity values, and vice versa [58, 62]. The aquifers' transmissivity (T) varies from 19.52 to 41.56 m^2/day, whereas hydraulic conductivity (K) values vary from (0.152 to 0.34 m/day) (Table 1). The aquifer's particular capacities have a significant role in the yield and discharge of the saturated aquifer, which varies from 2.33 gpm/ft to 8.0 gpm/ft (Table 1). The rate at which specific capacity increases or decreases reflects lithological change as well as groundwater flow. The abrupt lithological change might indicate a low-capacity aquifer system [64].

4.3 Aquifer system

Groundwater potential zones and the aquifer system's behavior were determined using hydrogeological features such as the thickness of subsurface lithology, geo-electrical layer, saturation zone thickness, and the types of aquifer comparison with borehole data. It is possible to use pumping test results to distinguish between various types of aquifers [65]. Clay layers serve as hydraulic barriers that separate aquifers because of their poor hydraulic conductivities [66]. During our research, we found that the aquifer was comprised of a mixture of unconsolidated material (clay, sand, and intermixed gravels and boulders) and bedrocks (lacustrine mudstone) (Fig. 2, 4, S1). This interpretation is based on Borehole data (PS-01, PS-02, PS-03, PS-04, PS-05) such as lithology, resistivity, and Spontaneous Potential (SP) well logs. Clay layers at a given depth serve as aquitards. Barriers between unconfined and constrained aquifers are formed by the low-permeability formation or layer [65, 66].

4.4

5. Discussion

5.1. Groundwater storage zone

According to Atangana [65], two kinds of aquifers have differing storativity values, which may be used to differentiate between them (values 0.000113–0.000213 range suggest storativity) (Table 1). From 0.01% to less than 1% of aquifer capacity may be attributed to confined wells. Although the specific yield (also known as storativity) of an unconfined aquifer is more than 0.01, this suggests that confined aquifers store water by extending their matrix and compressing water, both of which are often small in quantity [67].

The extremely impermeable clayey overburden protects the subterranean aquifer from contamination by surface runoff because of its high longitudinal conductivity (Abiola et al., 2009). The research area's centre and northeastern areas provide good protection with values between 0.29 and 0.65 mhos. The area's Northwestern and Southwestern sides have a week to poor protective capacity of 0.07–0.14 mhos (Table 4). Gravel, sand, and boulders are intermixed in low S levels, whereas mixed clay with gravel and sand is present in intermediate values. Protective layers may be formed when clay and silt are present in the stratum layer that lies under the aquifer. When present in high amounts, they form a protective cover [55]. The longitudinal conductance of low-resistivity materials varied from one VES point to the next, implying that the overall thickness of the materials changed [56, 57].

The transverse resistance associated with the unsaturated aquifer thickness is often greater than the transverse resistance associated with the saturated aquifer thickness in the absence of or with exceptionally low clay concentration [58]. Exceptionally high transverse resistance values relate to subsurface deposits that are very resistant [9]. Transverse resistance values may also be used to estimate the flow direction of groundwater in an aquifer. The total transverse resistance is one of the geoelectric properties used to define the major location of groundwater potential.

The high resistivity values are produced by intermixed sand, gravels, and boulders (23–120 ohm-m) [50]. Bedrock is exposed at higher altitudes, which may restrict currents from penetrating deeper (Fig. 1). According to Hodlur, Dhakate and Andrade [51], the low resistivity values are due to the presence of saturated sand and clay beneath the surface (Fig. 2). The boreholes PS-01 (36.3 m^2/day) and PS-01 (41.56 m^2/day) had the highest T values (Table 1). The high ratio of the T and K in the study area represents the coarser lithological material or the fractured zones [25, 26, 48]. In the subsurface potential zones, medium to fine intermixed clay, sand, and gravel material with moderate to low T values could be recommended. The various thickness differences of the groundwater potential zones might be determined from low to high T and K values [63].

5.2. 3D model of aquifer system

For the study area, a three-dimensional model of the subsurface aquifer system was developed (Fig. 6). The elevation and lithology variations on the surface and under the earth are shown in this geographical distribution model. (Fig. 6a-b) The highest heights, more than 670 m, are found in the south and southeast, while the eastern and northern regions are at a lower level, less than 380 m (Fig. 1b, 6a-b). Aquifer parameters were compared with five boreholes (BH-02, BH-02, BH-03, BH-04, and BH-05) drilled in typically elevated regions using the hydrological model. The shallow alluvial deposits have substantial lateral and vertical differences. Clay layers' act as aquitards between the saturated layers in the well-developed aquifer system (Fig. 6c). The presence of dry gravel and sands is associated with high resistivity levels in the borehole data and the VES subsurface resistivities five hydrological layers used as an indicator to estimate the groundwater potential zones (Fig. 6b) [50]. A similar condition was discovered in the Peshawar Basin (Fig. 6b-c), where thick clay layers divide unconfined and confined aquifer zones [33]. The Peshawar basin's aquifer system, which normally holds freshwater, is widely used.

Recent studies suggest that the aquifer system is comprised of three types of aquifers: unconfined, semi-confined, and confined. Alluvial to fluvial deposits in our study area are hydrogeological significant because of their inter-layered and diverse lithologies of clays, gravels, sands, and boulders [33]. Cornwell [38] reposted that the Peshawar basin is composed of thin, horizontally bedded sand, silt, and clay layers that are flooded in nature. Late Pleistocene lakes over the Peshawar basin were originally thought to have deposited these sediments [68, 69]. Because the sediments were accumulated by weathering and erosion in situ, they have a limited ability to be sorted by their composition [33]. Tube well data revealed the existence of an alluvial overburden aquifer system (Fig. 4).

The beginning depth of the restricted aquifer varies from well to borehole, ranging from 112 m to 130 m. Aquifers with a thickness of 24 to 110 m (Fig. 4, S1) can be found in the unconfined to semi-confined region. These aquifers were formed by the rapid deposition of coarser materials at high speeds, while the slower deposition of finer sediments was caused by variations in rainfall, topography, and streamflow [70]. Saturated aquifer types range from semi-confined to confined zones, and the borehole (PS-04) has a saturated thickness of up to 127 m. It has a transmissivity of 41.56 m²/day. According to this study, which confirms previous findings, the Bara River and rain feeds are the major sources of recharge for subsurface groundwater aquifers [71]. Freshwater is concentrated in the Peshawar basin's aquifer system. An ancient stream may have been submerged under more recent sediments, as suggested by these aquifer systems, according to Seong, Kang, Ree, Choi, Lai, Long and Yoon [72].6. Conclusions

This research was focused on groundwater potentiality and aquifer features from the Southern Peshawar region, which revealed fascinating geoelectrical and hydrogeological approaches. Hydrogeological potentially of the study was delineated by implementing the vertical electrical resistivity (VES), tube well data, pumping test analysis. During this study 13 VES and five Borehole data were used to assess the groundwater potential zone. Dar-Zarrouk parameters usually transverse resistance (TR), longitudinal conductance (S), and coefficient of Anisotropy (λ) show a variation in the distribution of aquifer system. Pumping test results show the transmissivity (T) and hydraulic conductivity (K) widely influenced on the rate of discharge and the type of aquifers. Aquifer system constitutes unconfined, semi-confined to confined nature with the beginning depth of the confined aquifer ranges from 112 m to 130 m, depending on the borehole. While the thickness of unconfined to semi-confined aquifers ranges from 24 m to 110 m, these aquifers are formed by the deposition of fine to coarser materials (clay, sand, gravels and boulders). Low impermeable alternative clay layers' act as aquitards with very low hydraulic conductivity. Aquifer system stores deep and enormous amount of groundwater with low to intermediate transmissivity and conductivity.

References

1. Woolway RI, Kraemer BM, Lenters JD, Merchant CJ, O'Reilly CM, Sharma S (2020) Global lake responses to climate change. Nat Reviews Earth Environ 1:388–403
2. Konapala G, Mishra AK, Wada Y, Mann ME (2020) Climate change will affect global water availability through compounding changes in seasonal precipitation and evaporation. Nat Commun 11:1–10
3. Hoogendam P, Boelens R (2019) Dams and Damages. Conflicting epistemological frameworks and interests concerning "compensation" for the Misicuni project's socio-environmental impacts in Cochabamba, Bolivia. Water 11:408
4. Farid A, Khalid P, Jadoon KZ, Jouini MS (2014) The depositional setting of the Late Quaternary sedimentary fill in southern Bannu basin, Northwest Himalayan fold and thrust belt, Pakistan. Environ Monit Assess 186:6587–6604
5. McArthur S, Allen D, Luzitano R (2011) Resolving scales of aquifer heterogeneity using ground penetrating radar and borehole geophysical logging. Environ Earth Sci 63:581–593
6. Olatunji S, Musa A (2014) Estimation of aquifer hydraulic characteristics from surface geoelectrical methods: case study of the Rima basin, North Western Nigeria. Arab J Sci Eng 39:5475–5487
7. Hermides D, Makri P, Kontakiotis G, Antonarakou A (2020) Advances in the Coastal and Submarine Groundwater Processes: Controls and Environmental Impact on the Thriassion Plain and Eleusis Gulf (Attica, Greece). J Mar Sci Eng 8:944
8. Makri P, Stathopoulou E, Hermides D, Kontakiotis G, Zarkogiannis SD, Skilodimou HD, Bathrellos GD, Antonarakou A, Scoullos M (2020) The Environmental Impact of a Complex Hydrogeological System on Hydrocarbon-Pollutants' Natural Attenuation: The Case of the Coastal Aquifers in Eleusis, West Attica, Greece. J Mar Sci Eng 8:1018
9. Utom AU, Odoh BI, Okoro AU (2012) Estimation of aquifer transmissivity using Dar Zarrouk parameters derived from surface resistivity measurements: A case history from parts of Enugu Town (Nigeria). J Water Resour Prot 4:993
10. Telford WM, Telford W, Geldart L, Sheriff RE (1990) *Applied geophysics*; Cambridge university press:
11. Okiongbo K, Akpofure E (2016) Hydrogeophysical characterization of shallow unconsolidated alluvial aquifer in Yenagoa and environs, Southern Nigeria. Arab J Sci Eng 41:2261–2270
12. Maliva RG (2020) Groundwater recharge and aquifer water budgets. In *Anthropogenic Aquifer Recharge*; Springer: ; pp. 63–102
13. Nag S, Ray S (2015) Deciphering groundwater potential zones using geospatial technology: a study in Bankura Block I and Block II, Bankura District, West Bengal. Arab J Sci Eng 40:205–214
14. Fetter C Upper Saddle River, New Jersey. *Applied Hydrogeology (4th ed.), Prentice-Hall, 598p* 2001
15. Nageswara Rao P, Appa Rao S, Subba Rao N (2018) Delineation of groundwater prospective zones from a delta region of India, using geoelectrical and water quality approach. Environ Earth Sci 77:1–16
16. Straface S, Yeh TC, Zhu J, Troisi S, Lee C (2007) Sequential aquifer tests at a well field, Montalto Uffugo Scalo, Italy.Water Resources Research43
17. Kowalsky MB, Finsterle S, Peterson J, Hubbard S, Rubin Y, Majer E, Ward A, Gee G (2005) Estimation of field-scale soil hydraulic and dielectric parameters through joint inversion of GPR and hydrological data. *Water Resources Research 41*
18. Perdomo S, Ainchil JE, Kruse E (2014) Hydraulic parameters estimation from well logging resistivity and geoelectrical measurements. J Appl Geophys 105:50–58
19. George N, Akpan A, Obot I (2010) Resistivity Study of Shallow Aquifers in theParts of Southern Ukanafun Local Government Area, Akwa Ibom State, Nigeria. E-J Chem 7:693–700
20. Al-Sabahi E, Rahim SA, Wan Zuhairi W, Al-Nozaily F, Alshaebi F (2009) The characteristics of leachate and groundwater pollution at municipal solid waste landfill of Ibb City, Yemen. Am J Environ Sci 5:256–266

21. George NJ, Ekanem AM, Ibanga JI, Udosen NI (2017) Hydrodynamic implications of aquifer quality index (AQI) and flow zone indicator (FZI) in groundwater abstraction: a case study of coastal hydro-lithofacies in South-eastern Nigeria. J Coastal Conserv 21:759–776
22. Zohdy AA, Eaton GP, Mabey DR (1974) Application of surface geophysics to ground-water investigations.5
23. Singh U, Das R, Hodlur G (2004) Significance of Dar-Zarrouk parameters in the exploration of quality affected coastal aquifer systems. Environ Geol 45:696–702
24. Olasehinde P, Bayewu O (2011) Evaluation of electrical resistivity anisotropy in geological mapping: A case study of Odo Ara, West Central Nigeria. Afr J Environ Sci Technol 5:553–566
25. Shahzad SM, Jianxin L, Shahzad A, Raza MS, Ya S, Meryem F (2018) Groundwater Potential Zone Identification in Unconsolidated Aquifer Using Geophysical Techniques around Tarbela Ghazi, District Haripur, Pakistan. Int J Geol Environ Eng 12:475–482
26. Khan S, Nisar UB, Ehsan SA, Farid A, Shahzad SM, Qazi HH, Khan MJ, Ahmed T (2021) Aquifer vulnerability and groundwater quality around Brahma Bahtar Lesser Himalayas Pakistan. Environ Earth Sci 80:1–13
27. Nisar UB, Khan MJ, Imran M, Khan MR, Farooq M, Ehsan SA, Ahmad A, Qazi HH, Rashid N, Manzoor T (2021) Groundwater investigations in the Hattar industrial estate and its vicinity, Haripur district, Pakistan: An integrated approach. *Kuwait Journal of Science 48*
28. Zhang J, Cliff D, Xu K, You G (2018) Focusing on the patterns and characteristics of extraordinarily severe gas explosion accidents in Chinese coal mines. Process Saf Environ Prot 117:390–398
29. Kaukab IS, Raza SH, Mahmood S (2018) Appraisal of surface deformation along Nanga Parbat Haramosh Massif through Remote Sensing and GIS Techniques. Pakistan Vis 19:1–11
30. Kazmi A, Jan M (1997) Graphic Geology and tectonic of Pakistan. publication. 130–141
31. Yeats R, Lawrence R (1982) Tectonics of the Himalayan thrust belt in northern Pakistan. In Proceedings of the US-Pakistan Workshop on Marine Sciences in Pakistan, ; pp. 177–200
32. Farid A, Khalid P, Jadoon KZ, Iqbal MA, Shafique M (2017) Applications of variogram modeling to electrical resistivity data for the occurrence and distribution of saline groundwater in Domail Plain, northwestern Himalayan fold and thrust belt, Pakistan. J Mt Sci 14:158–174
33. Muhammad S, Khalid P (2017) Hydrogeophysical investigations for assessing the groundwater potential in part of the Peshawar basin, Pakistan. Environ Earth Sci 76:1–12
34. Burbank D, Fort M (1983) Multiple episodes of catastrophic flooding in the Peshawar basin during the past 700,000 years. Geol Bull Univ Peshawar 16:43–49
35. Bibi M, Wagreich M, Iqbal S, Jan IU (2019) Regional sediment sources versus the Indus River system: the Plio-Pleistocene of the Peshawar basin (NW-Pakistan). Sed Geol 389:26–41
36. Gibling M, Tandon S, Sinha R, Jain M (2005) Discontinuity-bounded alluvial sequences of the southern Gangetic Plains, India: aggradation and degradation in response to monsoonal strength. J Sediment Res 75:369–385
37. Allen J (1964) Quaternary stratigraphic sequence in the Potwar basin and adjacent north west Pakistan. Geol Bull Univ Peshawar 1:2–5
38. Cornwell K (1998) Quaternary break-out flood sediments in the Peshawar basin of northern Pakistan. Geomorphology 25:225–248
39. Khan U, Janjuhah HT, Kontakiotis G, Rehman A, Zarkogiannis SD (2021) Natural Processes and Anthropogenic Activity in the Indus River Sedimentary Environment in Pakistan: A Critical Review. J Mar Sci Eng 9:1109
40. Tariq S (2001) Environmental geochemistry of surface and sub surface water and soil in Peshawar basin of NWFP Pakistan. *Unpublished PhD thesis, University of Peshawar*
41. Lutfi W, Sheikh L, Zhao Z, Song S, Qasim M, Rahim Y, Liu D, Wang Q, Zhu D-C, Zhang L-L (2021) The detrital zircon U-Pb-Hf isotopes of the Triassic sediments in northern Pakistan: Implications for crustal evolution of the NW Indian continent. Precambrian Res 357:106146
42. Jehangir S (1995) Modelling the hydrological impacts of land cover change in the Siran Basin, Pakistan. University of Leicester, United Kingdom)
43. Zhang H, Haan C, Nofziger D (1990) Hydrologic modeling with GIS: An overview. Appl Eng Agric 6:453–458
44. Stylianou II, Tassou S, Christodoulides P, Aresti L, Florides G (2019) Modeling of vertical ground heat exchangers in the presence of groundwater flow and underground temperature gradient. Energy Build 192:15–30
45. Pongmanda S, Suprapti A (2020) Performing application of cooper-jacob method for identification of storativity. In Proceedings of the IOP Conference Series: Earth and Environmental Science, ; p. 012128
46. Akhter G, Hasan M (2016) Determination of aquifer parameters using geoelectrical sounding and pumping test data in Khanewal District, Pakistan. Open Geosci 8:630–638
47. Suryoputro MR, Buana FA, Sari AD, Rahmillah FI (2018) Active and passive fire protection system in academic building KH. Mas Mansur, Islamic University of Indonesia. In Proceedings of the MATEC Web of Conferences, ; p. 01094
48. Khan U, Faheem H, Jiang Z, Wajid M, Younas M, Zhang B (2021) Integrating a GIS-based multi-influence factors model with hydro-geophysical exploration for groundwater potential and hydrogeological assessment: A case study in the Karak Watershed, Northern Pakistan. Water 13:1255
49. Mazáč O, Kelly W, Landa I (1985) A hydrogeophysical model for relations between electrical and hydraulic properties of aquifers. J Hydrol 79:1–19
50. Martínez J, Benavente J, García-Aróstegui J, Hidalgo M, Rey J (2009) Contribution of electrical resistivity tomography to the study of detrital aquifers affected by seawater intrusion–extrusion effects: the river Vélez delta (Vélez-Málaga, southern Spain). Eng Geol 108:161–168
51. Hodlur G, Dhakate R, Andrade R (2006) Correlation of vertical electrical sounding and borehole-log data for delineation of saltwater and freshwater aquifers. Geophysics 71:G11–G20

52. Nwachukwu S, Bello R, Balogun AO (2019) Evaluation of groundwater potentials of Orogun, South–South part of Nigeria using electrical resistivity method. Appl Water Sci 9:1–10
53. Hasan M, Shang Y, Jin W, Shao P, Yi X, Akhter G (2020) Geophysical Assessment of Seawater Intrusion into Coastal Aquifers of Bela Plain, Pakistan. Water 12:3408
54. Abiola O, Enikanselu P, Oladapo M (2009) Groundwater potential and aquifer protective capacity of overburden units in Ado-Ekiti, southwestern Nigeria. Int J Phys Sci 4:120–132
55. Alabi OO, Ojo AO, Akinpelu DF (2016) Geophysical investigation for groundwater potential and aquifer protective capacity around Osun State University (UNIOSUN) College of Health Sciences. Am J Water Resour 4:137–143
56. Falade AO, Oni TE, Oyeneyin A (2021) Intrinsic Parametric Approach to Groundwater Vulnerability Assessment: A Case Study of Ijero Mining Site, Ijero-Ekiti.
57. Yusuf M, Abiye T (2019) Risks of groundwater pollution in the coastal areas of Lagos, southwestern Nigeria. Groundw sustainable Dev 9:100222
58. Ponzini G, Ostroman A, Molinari M (1984) Empirical relation between electrical transverse resistance and hydraulic transmissivity. Geoexploration 22:1–15
59. Olayinka A, Oyedele E (2019) On the application of coefficient of anisotropy as an index of groundwater potential in a typical basement complex of Ado Ekiti, Southwest, Nigeria.Physical Science International Journal1–10
60. Bała M, Cichy A (2015) Evaluating electrical anisotropy parameters in miocene formations in the cierpisz deposit. Acta Geophys 63:1296–1315
61. Su B-Y, Yue J-H (2017) Research of the electrical anisotropic characteristics of water-conducting fractured zones in coal seams. Appl Geophys 14:216–224
62. Rasool U, Chen J, Muhammad S, Siddique J, Venkatramanan S, Sabarathinam C, Siddique MA, Rasool MA (2020) Geoinformatics and geophysical survey-based estimation of best groundwater potential sites through surface and subsurface indicators. Arab J Geosci 13:1–17
63. Chukwudi CE (2011) Geoelectrical studies for estimating aquifer hydraulic properties in Enugu State, Nigeria. Int J Phys Sci 6:3319–3329
64. Bourel B, Barboni D, Shilling AM, Ashley GM (2021) Vegetation dynamics of Kisima Ngeda freshwater spring reflect hydrological changes in northern Tanzania over the past 1200 years: Implications for paleoenvironmental reconstructions at paleoanthropological sites. Palaeogeogr Palaeoclimatol Palaeoecol 580:110607
65. Atangana A (2017) *Fractional operators with constant and variable order with application to geo-hydrology*, Academic Press:
66. Kirsch R (2006) *Groundwater geophysics*; Springer: ; Volume 493
67. Worthington SR, Foley AE (2021) Development of spatial permeability variations in English chalk aquifers.Geological Society, London, Special Publications*517*
68. Kothyari GC, Pant P, Talukdar R, Taloor AK, Kandregula RS, Rawat S (2020) Lateral variations in sedimentation records along the strike length of north Almora thrust: central Kumaun Himalaya. Quaternary Sci Adv 2:100009
69. Haneef M, Jan MQ, Rabbi F (1986) Fracture fills or sedimentary dykes in the lake sediments of Jalala, NWFP, a preliminary report. Geol Bull Univ Peshawar 19:151–156
70. Whipple K, Gasparini N (2014) Tectonic control of topography, rainfall patterns, and erosion during rapid post–12 Ma uplift of the Bolivian Andes. Lithosphere 6:251–268
71. Eldaw E, Huang T, Mohamed AK, Mahama Y (2021) Classification of groundwater suitability for irrigation purposes using a comprehensive approach based on the AHP and GIS techniques in North Kurdufan Province, Sudan. Appl Water Sci 11:1–19
72. Seong YB, Kang H-C, Ree J-H, Choi J-H, Lai Z, Long H, Yoon HO (2011) Geomorphic constraints on active mountain growth by the lateral propagation of fault-related folding: A case study on Yumu Shan, NE Tibet. J Asian Earth Sci 41:184–194

Tables

Table 1: Data from pumping tests and parameters of the groundwater aquifer.

Age	Formations	Lithology
Late Triassic to Jurassic	Nikanai Ghar Formation	Thick-finely, coarsely dolomitic marble and crystalline marble
Triassic	Kashala Formation	Brown weathered marble and dolomitic marble alternating and calcareous phyllite
Permian	Karapa Greenschist	Green schist (metamorphosed tholeiitic basalt)
Carboniferous	Jafar Kandao Formation	conglomerate composed of pebbles and cobbles of quartzite, argillite, or limestone in argillite or quartzite matrix.
Devonian	Nowshera Formation	sandy dolomite, calcareous argillite, calcareous and dolomitic quartzite, and fossiliferous limestone
Silurian	Panjpir Formation	Interbedded argillite and fossiliferous limestone and dark gray to olive-gray argillite, phyllite, and meta-siltstone.
Ordovician	Misri Banda Quartzite	Quartzite
Cambrian	Ambar Formation	Quarzitic dolomite
Paleo-Proterozoic	Tanawal Formation	quartzite, speckled quartzite, phyllite, argillaceous sandstone, quartzose sandstone, shale and quartzose conglomerate.
Meso-Proterozoic	Hazara Formation	argillite, claystone, limestone, greywacke sandstone, siltstone, shale.

Table 2: Subsurface lithology and VES data are compared.

Well Name	Saturated zone thickness (m)	Aquifer thickness (m)	Water Table (m)	Casing diameter (m)	Pumping Test Data					Jacobs's Pumping Method	
					Draw Down		Discharge (m^3/day)	Specific Capacities (gpm/ft)	Transmissivity (m^2/day)	Hydraulic conductivity (m/day)	Storativity
					(m)	(ft)					
P-01	128	74	24.4	0.254	7.6	25	364	2.66	19.52	0.152	0.000125
P-02	140	55	39.62	0.254	9.1	30	381.57	2.33	21.58	0.154	0.000154
P-03	107	64.5	53.52	0.254	3.05	10	408.824	7.5	36.30	0.34	0.000213
P-04	127	68	23.2	0.254	4.57	15	654.119	8	41.56	0.32	0.000281
P-05	110	60	51.82	0.254	6.09	20	390.654	3.6	24.41	0.22	0.000113

Table 3: Shows the Dar Zarrouk parameters and aquifer thickness based on VES data.

Resistivity (ohm-m)	lithology
15-85	Dry Sediments
17-40	Saturated clay
23-120	sand, gravels, and boulder
30-50	Lose shale

Table 4: Depicts the aquifer's protective capacity in terms of longitudinal conductance.

VES. no.	Resistivity (Ohm.m)						Thickness of subsurface layers (m)						Water table	Transverse resistance ($Ohm.m^2$)	longitudinal conductance (Siemens)
	p1	p2	p3	p4	p5	p6	h1	h2	h3	h4	h5	h6	(m)		
1	39.1	19.5	47.1	23.8	37.1	-	6.14	40.9	36.3	68.6	-	-	49.8	4380.03	0.9120
2	70.01	175.5	44.44	25.99	55.5	-	2.886	3.803	6.646	94.83	-	-	43.8	3629.46	0.2912
3	103.8	15.44	13.84	19.71	53.86	16.16	0.427	2.1	0.658	5.45	31.6	52	50.2	2735.57	0.4140
4	12.7	37	83.2	11.7	17.4	54.1	2.38	9.46	15.3	29.5	97	21	37.4	4822.26	0.8081
5	15	6.87	14.8	22.4	45.1	-	3.15	14.5	34.7	73.2	-	-	34.2	2300.11	1.2052
6	78.4	13.6	23.4	49.4	34.2	-	9.75	8.09	34.7	51.2	-	-	38.9	4215.68	0.5213
7	848	612.6	127	87.94	119.2	251.8	1.2	5.239	20.25	37.44	59.28	23	51.2	22948.81	0.0715
8	109.5	35.29	13.09	30.1	42.4	-	0.7995	8.608	37.89	85.64	31.5	-	45.8	4800.67	0.7138
9	63.8	13.4	77.3	10.5	26.4	-	1.25	1.4	2.69	43	79.1	-	45.6	2846.19	0.6658
10	65.24	28.09	23.3	18.12	216.4	175.4	1.177	1.22	3.811	5.221	7.52	56.2	31.5	11779.27	0.1427
11	110.6	130.1	219.2	135.5	238	94.44	1.321	1.548	12.42	22.34	22.69	71.6	47.8	18259.16	0.1422
12	47.2	102	67.3	25.8	45.2	-	1.4	2.4	17.3	45.821	45.1	-	22.4	4695.87	0.3896
13	23.5	8.31	68.954	83.3	170	-	1.9	2.07	28.21	39.65	71.62	-	44.7	17485.29	0.4052

Table-5

Longitudinal conductance (mhos)	Protective capacity rating
>10	Excellent
5–10	Very good
0.7–4.9	Good
0.2–0.69	Moderate
0.1–0.19	Weak
<0.1	Poor

Figures

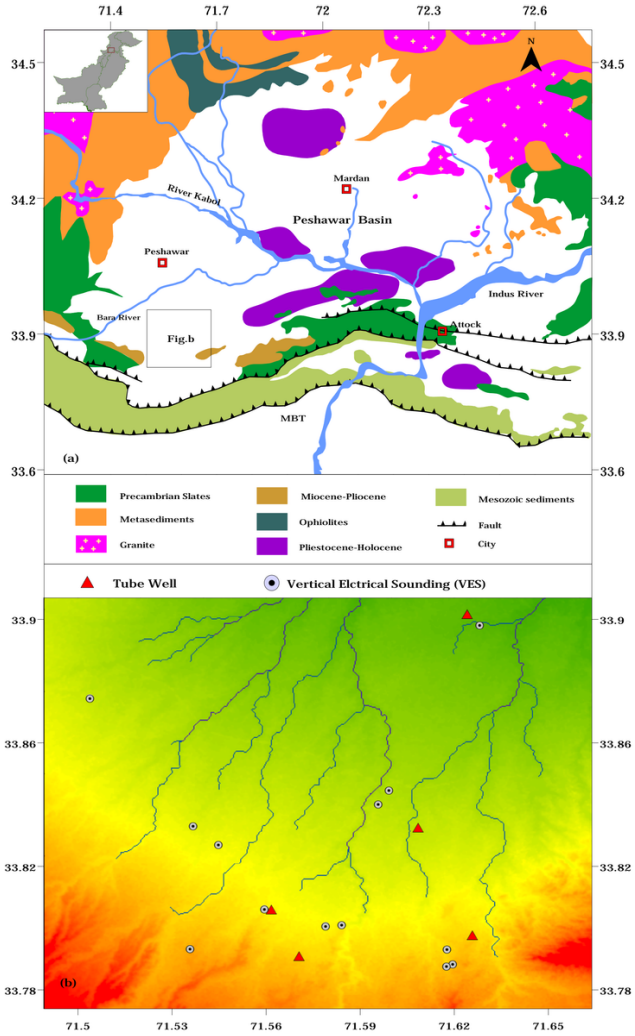

Figure 1

Base map of the study area (a) Geological map of the Peshawar Basin and surroundings; (b) research area map, with circles indicating VES sites and solid red triangles indicating drill positions.

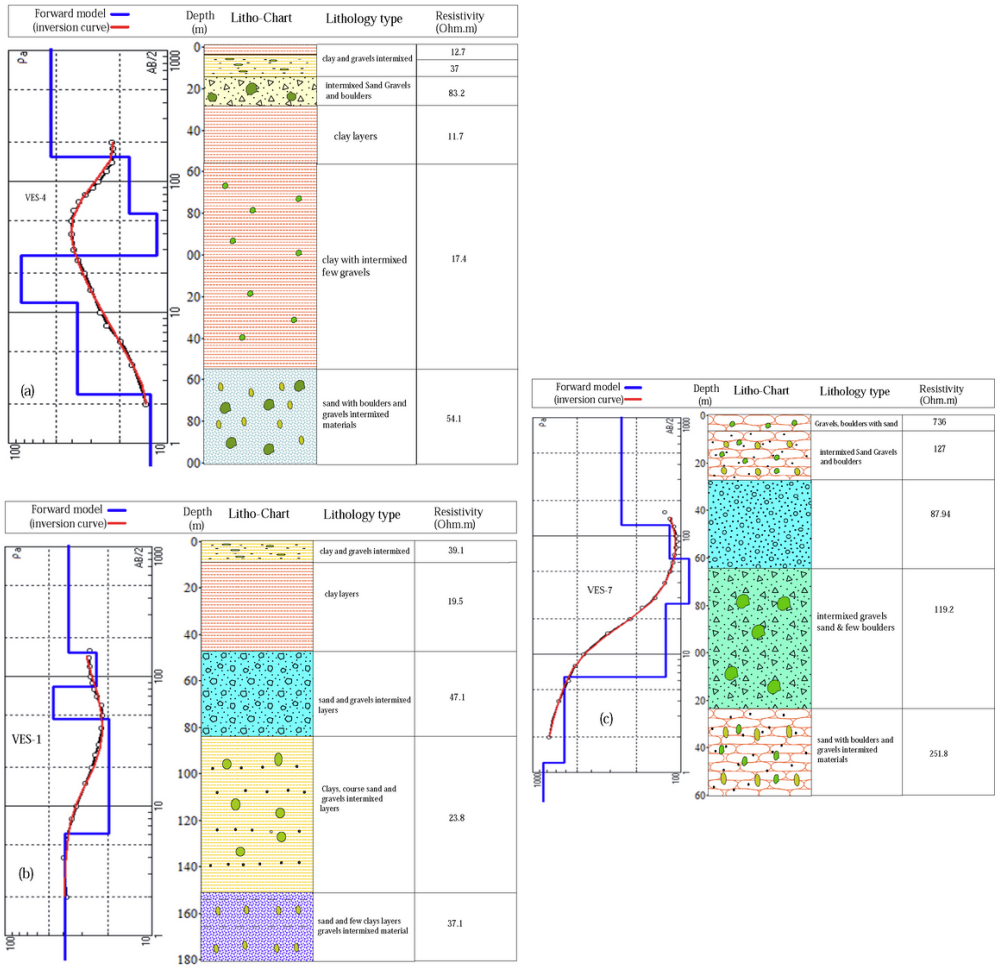

Figure 2

Represents the VES data inversion and forward model results comparison with electro-stratigraphic model.

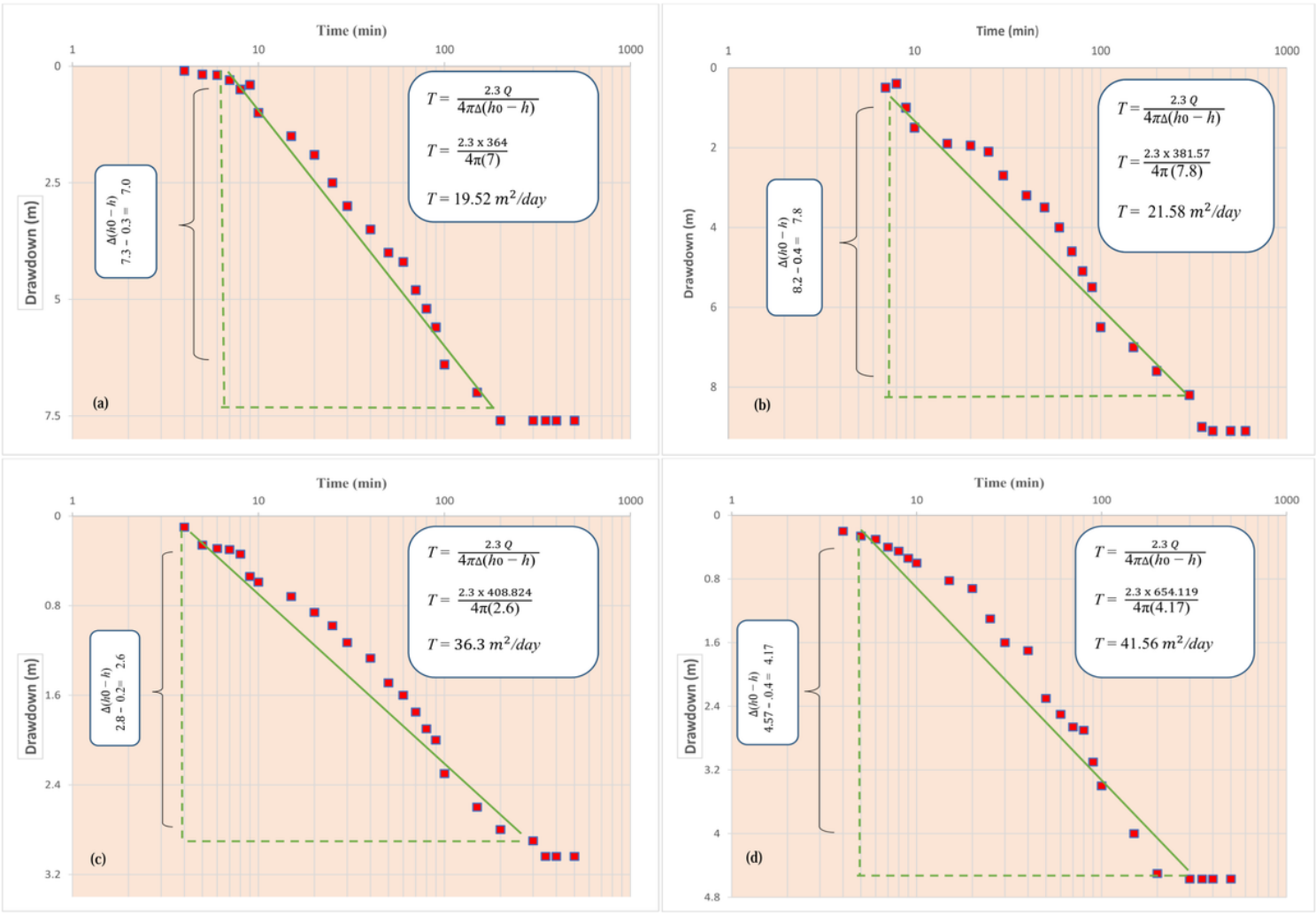

Figure 3

The pumping test analysis approach was used to estimate the borehole transmissivity (PS-01, PS-02, PS-03, PS-04, and PS-05).

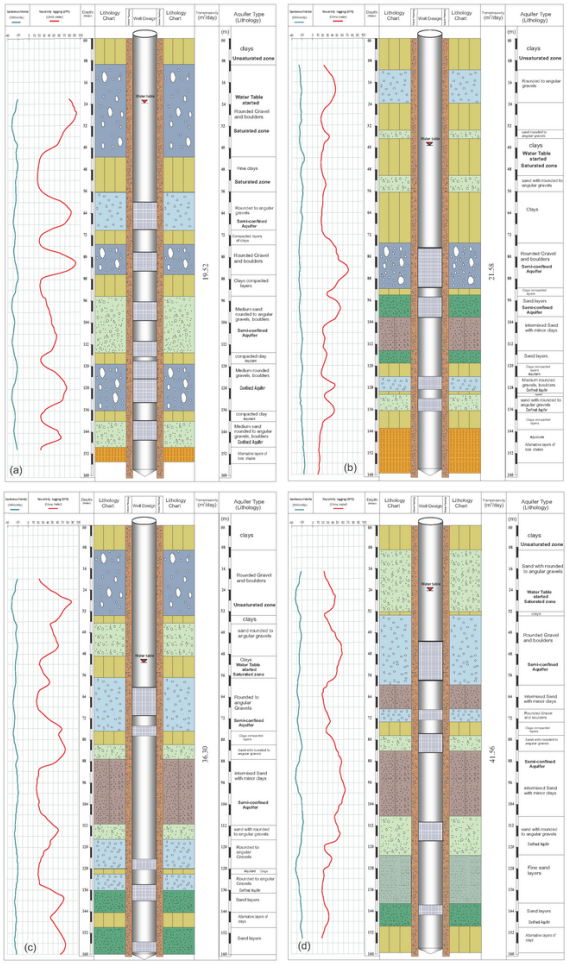

Figure 4

Borehole data (PS-01 to PS-04) (a-d) Shows the depth logs, such as the resistivity log (SPR), spontaneous potential log (SP), lithological chart, aquifer types, and the transmissivity of each borehole, in relation to the tube well design.

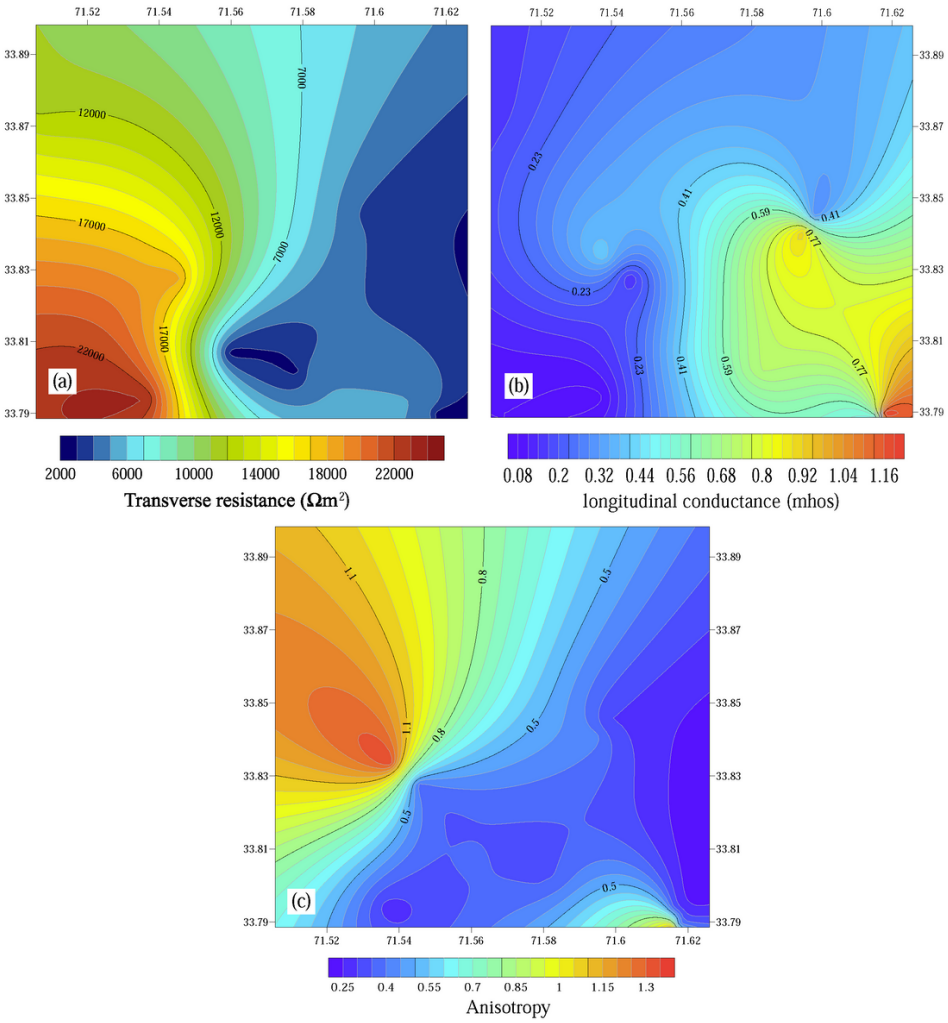

Figure 5

Relief map of the Dar Zarrouk parameters. (a) Estimated transverse resistance map for the region's layer overlain aquifer. (a) map of Longitudinal conductance, (c) anisotropy relief map of this study aquifer region.

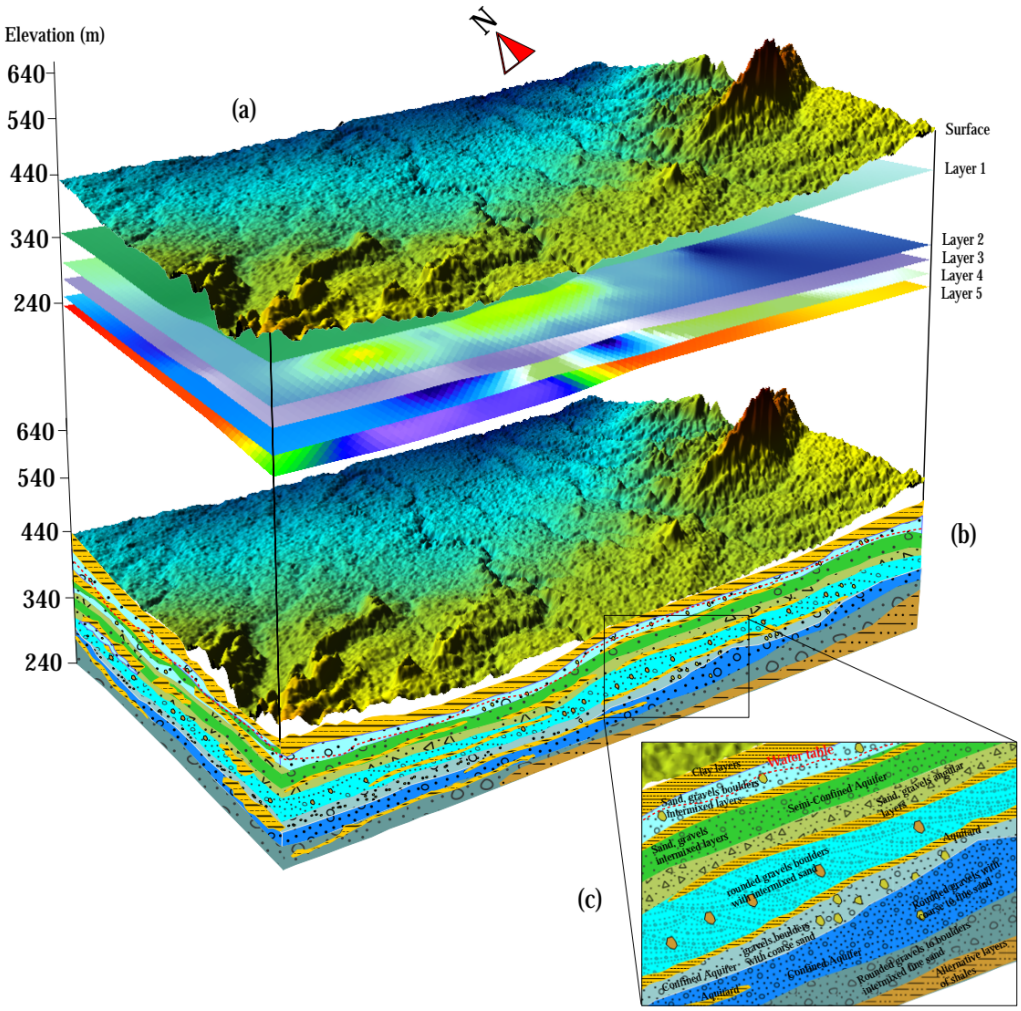

Figure 6

Borehole and VES data sets were used to create a 3D surface elevation and subsurface lithological model of the research region. (a) Aquifer resistivity layers and surface elevation about subsurface depth; (b) aquifer hydrogeological model; (c) subsurface lithological face from unsaturated to the saturated zone of the aquifer system and aquifer types.

Supplementary Files

This is a list of supplementary files associated with this preprint. Click to download.

- AppendexA1.pdf